CHAPTER 5

APPLICATION OF PURE ZnO AND WO_3-DOPED ZnO FOR USE AS PHOTOVOLTAIC DEVICES

5.1 Introduction

It is expected that the global energy demand will double within the next 50 years. Fossil fuels, however, are running out and held responsible for the increased concentration of CO_2 in the earth's atmosphere. Hence, developing environmentally friendly, renewable energy is one of the challenges to society in the 21st century. One of the renewable energy technologies is photovoltaic, the technology that directly convert daylight into electricity. Photovoltaic is one of the fastest growing industries of all the renewable energy technologies [1]. Solar cell manufacturing based on the technology of crystalline, silicon devices is growing by approximately 50% per year and this growth rate is increasing [1].

Solar cells comprising of an inorganic semiconductor have found markets for small scale devices such as solar panels on roofs, pocket calculators and water pumps. These conventional solar cells can harvest up to as much as 24% [2] of the incoming solar energy which is already close to the theoretically predicted upper limit of 30% [2, 3]. This illustrates that technologies which allow low fabrication costs, rather than somewhat higher conversion efficiencies, are now desired. One approach here would be to reduce the amount of silicon by using thinner films on (cheap) glass substrates. Today, the production of these solar cells still requires many energy intensive processes at high temperatures (400-1400 °C) and high vacuum conditions with numerous lithographic steps leading to relatively high manufacturing costs [4].

Another interesting alternative to inorganic cells is given by the semiconducting polymers, which combine the optoelectronic properties of conventional semiconductors with the excellent mechanical and processing properties of polymeric i.e. "plastic" materials. These can be processed from solution at room-temperature onto e.g. flexible substrates using simple and therefore cheaper deposition methods like spin or blade coating. Therefore, these materials could generate the prospect of cheaper production using large area devices and the use of flexible substrates.

Polymer organic solar cells often use a nanostructured interpenetrating network of electron-donor and electron-acceptor materials [5-7]. This bulk-heterojunction morphology enhances the interfacial area were the photogenerated excitons are dissociated into charge carriers and enables holes and electrons to be transported and collected. Various bulk-heterojunction photovoltaic devices have been made in recent years using polymer composites [5] or conjugated polymers with fullerenes [6, 8-10]. Moreover, polymers have been blended with CdSe nanoparticles to create hybrid solar cells [11-12]. These hybrid polymer-inorganic solar cells utilize the high electron mobility of the inorganic phase to overcome charge-transport limitations associated with organic materials. In addition, efficient bulk-heterojunction solar cells can be made using ZnO nanoparticles and a conjugated polymer [13]. These cells can be processed from solution and exhibit an incident photon to current conversion efficiency up to 0.9%. The environmentally friendly and low-cost ZnO offers a new perspective towords 'green electricity'.

In contrast to silicon and most conventional inorganic semiconductors, photoexcitation of organic semiconductors does not directly result in free charge carriers. Instead, a strongly bound electron-hole pair or exciton, is generated. This exciton can be separated to form free charge carriers at the interface between an electron-donor (n-type) and electron-acceptor (p-type) material. In general, the exciton lifetime and mobility within organic semiconductor are limited by radiative and non-radiative decay; so only excitons generated in close vicinity of a p-n interface will give rise to charges. In bulk-heterojunction solar cells, this limitation is circumvented by intimately mixing the p- and n-type materials, creating junctions throughout the bulk of the material and ensuring quantitative charge generation from photogenerated excitons. High charge-carrier mobilities are advantageous to effectively collect these charges and prevent charge recombination. Hybrid nanocomposite mixtures can combine the advantages of both types of materials: the solution processing of organic semiconductors and the high charge-carrier mobility of inorganic semiconductors. The effectiveness of the use of nanostructured interfaces for photovoltaic applications is most vividly demonstrated by the high efficiencies obtain by dye-sensitized photoelectrochemical cells [14-15]. However, the use of electrolyte in this type of cell imposes serious technological complications. Hybrid bulk-heterojunction cells allow easier processing, and promising efficiencies have already been obtained by combining nanoparticles such as CdSe and ZnO with a polythiophene conjugated polymer [11].

ZnO nanocrystalline can be introduced as the n-type semiconductor in hybrid bulk-heterojunction solar cells as it is a cheap and environmentally friendly material that can be synthesized in high purity and crystallinity. ZnO has high electron

mobility, even when measured on films consisting of assembled ZnO nanoparticles [16].

5.1.1 Electrical characteristic parameter of the photovoltaic

Solar cells are further characterized by measuring the current-voltage curve under illumination of a light source that mimics the sun spectrum. A typical current-voltage curve of a bulk-heterojunction cell is shown in Figure 5.1(a). Since organic semiconductors show very low intrinsic carrier concentration, the metal-insulator-metal (MIM) model [17] seems to be best suited to explain this characteristic. The characteristic points used to characterize a solar cell are labeled in Figure 5.1(a). In addition, for each of these points, the energy diagram for a single-layer cell with an indium-tin-oxide (ITO) anode and aluminum cathode is displayed.

In Figure 5.1 (b) a semiconductor, sandwiched between two metal electrodes with different work functions is depicted for several situations. The metals are represented by their Fermi levels, whereas for the semiconductor the valence and conduction bands, corresponding to the molecular LUMO (lowest unoccupied molecular orbital) and the HOMO (highest occupied molecular orbital) levels, are shown. In Figure 5.1 (b-a), there is no voltage applied (i.e., short-circuit conditions). Hence, there is no net current flowing in the dark, and the built-in electric field resulting from the difference in the metals' work functions is evenly distributed throughout the device. Under illumination, separated charge carriers can drift in this electric field to the respective contacts: the electrons move to the lower work function metal and the holes to the opposite. The device then works as a solar cell [17].

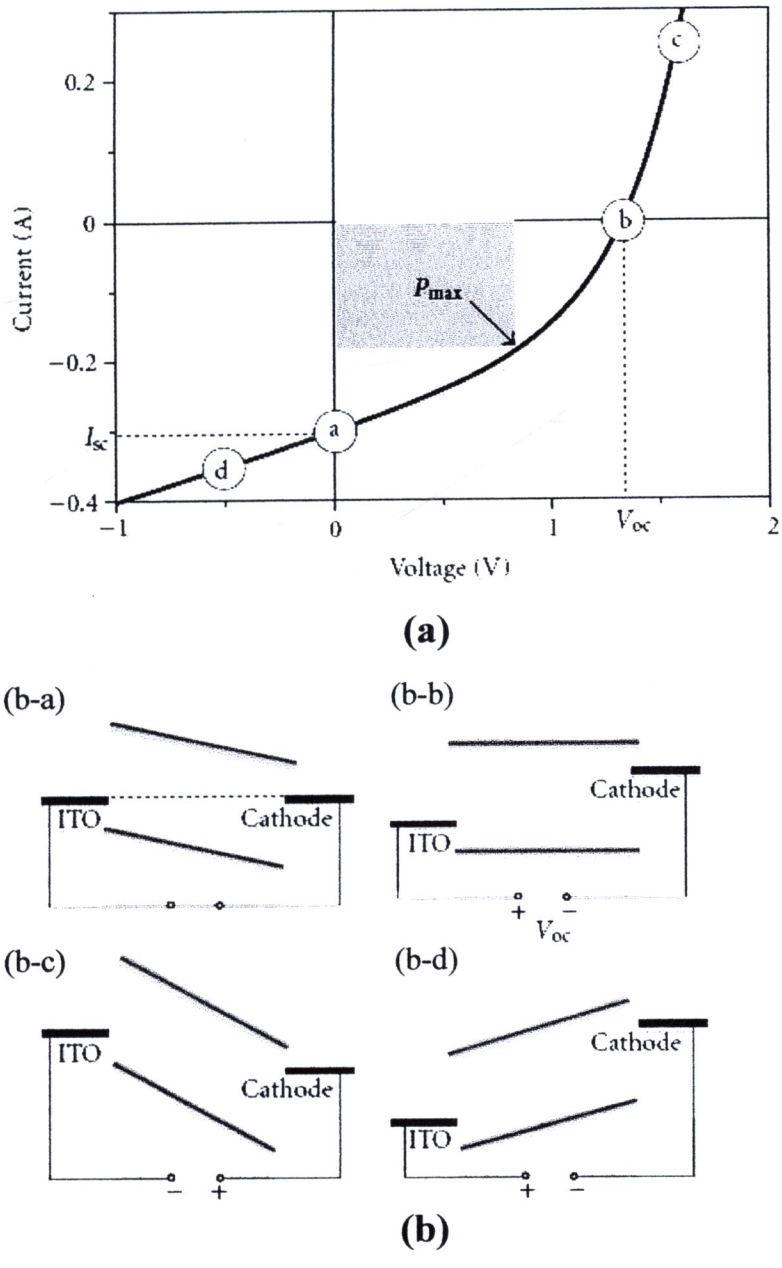

Figure 5.1 (a) Current (voltage) characteristics of a typical organic diode (b) Metal-insulator-metal picture of organic diode device function. (b-a) Closed circuit condition: under illumination photogenerated charges drift toward the contacts. (b-b) Open circuit condition: the current becomes zero. (b-c) Reversed bias: photogenerated charges drift in strong electric fields, the diode operates as a photodetector. (b-d) Forward bias larger than V_{OC}: the injection increases and the diode open up [17].

In Figure 5.1 (b-b), the situation is shown for open circuit conditions, also known as "flat band condition". The applied voltage is called the open circuit voltage (V_{OC}), which corresponds in this case to the difference in the metals' work functions and balances the built-in field. As there is no net driving force for the charge carriers, the current is zero. In Figure 5.1 (b-c) the situation is shown for an applied reverse bias and only a very small injected dark current (j_0) can flow. Under illumination, the generated charge carriers drift under strong electric fields to the respective electrodes and the diode works as a photodetector. If a forward bias larger than the open circuit voltage is applied as shown in Figure 5.1 (b-d), the contacts can efficiently inject charges into the semiconductor. If these can recombine radiatively, the device works as a LED. The asymmetric diode behavior results basically from the different injection of the two metals into the HOMO and LUMO levels, respectively, which depends exponentially on the energy barrier between them.

Therefore, the parameters including the short-circuit current, the open-circuit voltage, the fill factor and the power conversion efficiency were used for photovoltaic characterization. In these parameters are indicated on a current-voltage curve of a solar cell under illumination that could summarize below.

5.1.1.1 Short-circuit current [18]

The short circuit current (I_{SC}) is the current in the illuminated device at 0 V bias. The amount of current is determined by the overlap between the absorption spectrum of the photovoltaic and solar spectrum, the intensity of the sunlight, the thickness of the active layer and the excitation/charge collection efficiency.

5.1.1.2 Open-circuit voltage [18]

The open-circuit voltage (V_{OC}) is the voltage represents the bias which have to be applied in devices in order to decimate the current generated by the illumination of our device. So, at the V_{OC} point there are no external current which flowing through the device under illumination (I= 0 A)

5.1.1.3 Fill factor (FF) [18]

The purpose of photovoltaic is to deliver power (current x voltage). The fourth quadrant of the current-voltage curve shows where the cell can deliver power. In this quadrant a point can be found at which the power reaches its maximum, called the maximum deliverable power, the maximum power point, versus the theoretical maximum power ($P_{theor\ max}$), the product of V_{OC} and I_{SC}

$$FF = \frac{P_{\max}}{P_{theor\ \max}} = \frac{I_{\max} \cdot V_{\max}}{I_{SC} \cdot V_{OC}} \tag{5.1}$$

It is a measure for diode properties of the photovoltaic. The higher the number, the more ideal the diode is. The quality of the diode can be negatively affected by series and shunt resistances, second diode effects and non-linear effects like bulk and surface injection dependent recombination velocities.

5.1.1.4 Power conversion efficiency [18]

The power conversion efficiency (η) reflects how good the photovoltaic can convert light to electrical current. It is ratio of delivered power to the irradiated light power (P light).

$$\eta = \frac{P_{\max}}{P_{light}} = \frac{I_{SC} \cdot V_{OC} \cdot FF}{P_{light}} \tag{5.2}$$

5.1.2 The ZnO nanoparticles as an electron acceptor with an electron donor conjugated polymers P3HT

In this research, hybrid photovoltaic devices were fabricated using ZnO nanoparticles as an electron acceptor and conjugated polymers P3HT as an electron donor. P3HT always be chosen as an electron donor in bulk heterojunction because of its high carrier mobility [19-20]. The excitons of these devices, created after the light absorption of P3HT, had to diffuse towards this charge-transfer interface for charge generation to occur. The diffusion length of the excitons, however, was typically 10 nm or less. This means that for efficient charge generation after absorption of light, each exciton had to find a donor-acceptor interface within a few nm, otherwise it will be lost without charge generation. Therefore, the hybrid bulk heterojunction devices are much more sensitive to the nanoscale morphology in the blend.

The injection and photovoltage critically of hybrid bulk heterojunction solar cell depend on the interfaces with the electrodes. Generally, the contact resistance becomes smaller, the smaller the injection barriers at either electron or hole collecting electrodes are. Interfacial layers are often proposed for the lowering of these barriers as shown by the insertion of an ultrathin (<1 nm) layer of LiF between the metal cathodes and the active layer in photovoltaic devices, which resulted in a lower cathode work function [21]. On the other side, the ITO work function could be increased by introduction of a layer of poly(3,4-ethylenedioxythiophene):poly (styrenesulfonate) (PEDOT: PSS). Therefore, this PEDOT:PSS layer could improve the performance of hybrid photovoltaic [22].

The poly(3-hexylthiophene) (P3HT) has highest occupied molecular orbital (HOMO) equal to 5.2 eV and lowest unoccupied molecular orbital (LUMO) equal to 3.3 eV [20], while ZnO nanoparticles have a valence band equal to 7.6 eV and

conduction band equal to 4.4 eV [23]. Moreover, the LUMO of PEDOT: PSS is 5.0 eV [23]. All of these values are relative to the vacuum level. The chemical structure of P3HT and PEDOT:PSS were shown in Figures 5.2(a) and 5.2(b), respectively. Exciton dissociation of P3HT/ZnO hybrid bulk-heterojunction that was deposited on an ITO substrate with PEDOT:PSS layer and capped with Al as a metal back electrode, was shown in Figure 5.3.

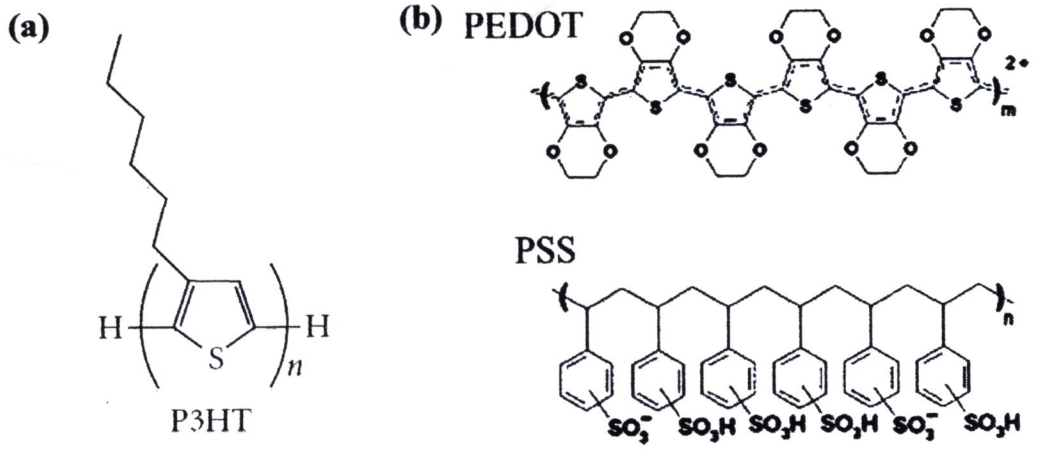

Figure 5.2 Chemical structures of (a) P3HT and (b) PEDOT:PSS [24]

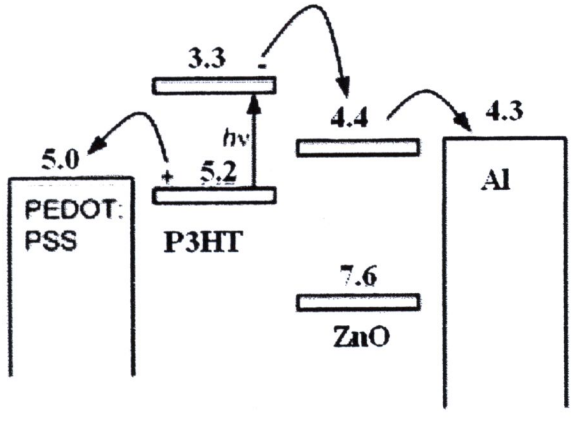

Figure 5.3 Exciton dissociation of P3HT/ZnO hybrid bulk-heterojunction [20, 23]

5.1.3 Literature review

In 1996, The processes of charge separation and transport in hybrid bulk heterojunction solar cells using cadmium sulfide nanocrystals and the conjugated polymer poly (2-methoxy,5-(2'-ethyl)-hexyloxy-*p*-phenylenevinylene) (MEH-PPV) as active layer was investigated by Greenham et al. [25] It was found that phase segregation of these photovoltaic devices using the composite was crucial in providing paths for both electrons and holes to travel to the appropriate electrode without recombination. The use of nanocrystals allows great flexibility in controlling the performance of photovoltaic devices, since both the electronic energy levels and the morphology of the composite materials may be altered by changing the nanocrystal size, concentration, and surface ligand. The energy conversion efficiency of these devices was 0.2% under Air Mass (AM) 1.5 conditions that was a typical solar spectrum.

In 2004, nanocrystalline ZnO prepared by hydrolysis and condensation method was used as the n-type semiconductor in hybrid bulk-heterojunction photovoltaic by Janssen et al. [23]. The device structure consisted of an 80 nm thick MDMO-PPV (poly[2-methoxy-5-(3',7'-dimethyloctyloxy)-1,4phenylenevinylene]) :ZnO blend, sandwiched between PEDOT:PSS and an aluminum top electrode (Glass/PEDOT : PSS/MDMO-PPV:ZnO/Al). It was found that these devices showed a power conversion efficiency (η) = 1.6% at 1 sun equivalent.

In 2006, hybrid polymer–metal oxide bulk-heterojunction solar cells were constructed by Janssen et al. [13]. The active layer of this device was fabricated by blending nanocrystalline zinc oxide nanoparticles prepared by hydrolysis and condensation method and regioregular poly(3-hexylthiophene) (P3HT). Thermal annealing of the spin-cast films and appropriate amount of ZnO in the blend

significantly improved the solar-energy conversion efficiency (η) of these hybrid solar cells to ≈ 0.9 % under Air Mass (AM) 1.5 conditions.

In 2005, a TiO_2 interconnected network structure for photovoltaic applications, which was obtained using polystyrene-block-polyethylene oxide diblock copolymer as the templating agent was fabricated by Wang et al. [26]. The synthesis method was simple and highly reproducible. The pore size of the structure was controlled by the amount of Ti precursor provided. The heterojunction solar cells consisting of a TiO_2 porous network structure and MEH-PPV showed power conversion efficiency (η) of 0.29%.

In 2007, Ohkita et al. [27] modified the metal oxide sufface with dye molecules in organic-inorganic hybrid solid solar cells by using double layered cells consisting of P3HT and a flat layer of dense TiO_2. The additional increase showed that the chemical modification with dye molecules could serve not only as a photosensitizer but mainly as an energy funnel and/or an electronic mediator to significantly improve the electron injection efficiency from P3HT to TiO_2. The highest of power conversion efficiency (η) in this work was 0.24%.

Moreover, ZnO could use as optical spacer in polymer solar cells. This application of ZnO was reported by Jansen et al. in 2007 [28]. ZnO layer was inserted between the active layer (P3HT:PCBM) and the reflective electrode results in a redistribution of the optical electric field. The increased photocurrent of P3HT:PCBM solar cells with an additional ZnO layer was caused by enhanced light absorption as a result of redistribution of the optical electrical field inside the device. The absorption was significantly enhanced for thin (60 nm) films. For thicker absorbing layers, the effect of the optical spacer was less pronounced, and may either enhance or decrease light absorption, depending on the thickness of the relevant layers.

5.2 Experimental

5.2.1 Chemical

Hybrid bulk heterojunction photovoltaic devices based on pure ZnO and WO_3-doped ZnO were prepared using the chemicals as follows:

- Chlorobenzene (Sigma-Aldrich, 99.99%, HPLC, United States)
- Chloroform (Sigma-Aldrich, 99.99%, HPLC, United States)
- Acetone (Sigma-Aldrich, ≥99.5%, A.S.C., United States)
- Isopropyl Alcohol (Aldrich, 99.5%, HPLC, United States)
- Poly(3,4-ethylenedioxythiophene):poly(styrenesulfonate) (PEDOT:PSS) (Baytron P, 99.99%, United States)
- Poly(3-hexylthiophene) (P3HT) (Sigma-Aldrich, 99.99%, United States)
- 1-(3-methoxycarbonyl)propyl-1-phenyl[6,6]C_{61} (PCBM) (Sigma-Aldrich, 99.99%, United States)
- Lithium fluoride (LiF) (Aldrich, 99.99%, United States)
- Aluminum (Al) (Sigma-Aldrich, 99.99%, United States)

5.2.2 Apparatus

Hybrid bulk heterojunction photovoltaic devices based on pure ZnO and WO_3-doped ZnO were tested using the equipment as follows:

- 200 Watt Solar Simulator (ORIEL, United States)
- Source-Measure Unit (Keithley 236, United States)
- Evaporator (Denton Vacuum, DV 502, United States)
- Vacuum Oven (Fisher model 281, United States)

- Ultra-Violet Ozone cleaning System (UVOCS model T16X16/OES, United States)
- Glove Box (Vacuum Atmospheres Company (VAC), United States)
- Spincoater (Specialty Coating System model P6700, United States)

5.2.3 Measurement conditions

Since the efficiency is temperature excitation therefore spectrum, illumination intensity dependence and test conditions were designed to obtain meaningful and comparable values. Standard test conditions include measurement at 25 °C under 100 mW/cm^2 of Air Mass (AM) 1.5 irradiation (Oriel). The AM 1.5 is the spectrum of the 1 sun equivalent as shown in Figure 5.4, which can be considered to be a blackbody radiation at 5800 K, attenuated for scattering and absorption in the atmosphere. The system's solar mismatch factor of 10% was determined using a calibrated standard diode. The system was independently compared with a NREL certified simulator. Current-voltage characteristics were collected using Keithley 236 source-measurement unit.

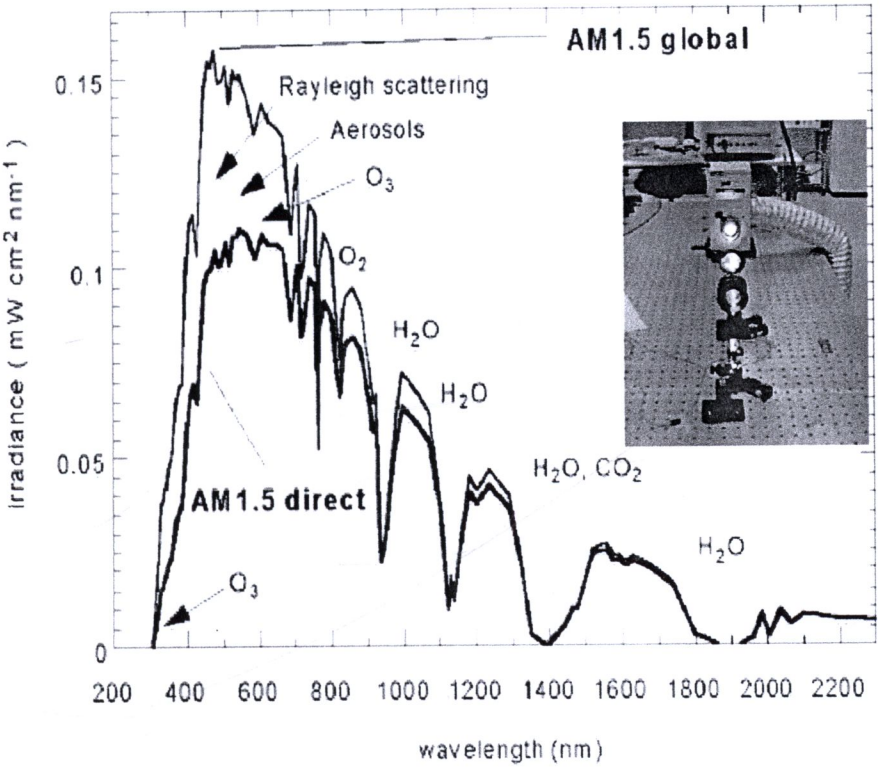

Figure 5.4 The AM 1.5 solar spectrum with total irradiation power 100 mW/cm^2. Inset shows the solar simulation system [2].

5.2.4 Preparation of photovoltaic devices

5.2.4.1 Indium Tin Oxide (ITO) glass cleaning

- ITO glasses (Delta Technologies R_s=10 Ωsq^{-1}) were prepared with the size of 25mm x 25mm.
- ITO glasses were cleaned by acetone in an ultrasonic bath for 20 min.
- ITO glasses were cleaned again by isopropyl alcohol in an ultrasonic bath for 20 min.
- These glasses were dried in a vacuum oven at 80 °C for 30 min.
- These glasses were cleaned in the Ultraviolet Ozone cleaning for 90 min.

5.2.4.2 ZnO/P3HT solution preparation

- 30 mg of ZnO nanoparticles and WO_3-doped ZnO with different WO_3 concentrations including 0.25, 0.50, 0.75, 1.0 and 3.0 mol% were dispersed in 1 mL of methanol and chlorobenzene solution in the ratio of 15:85 by volume.
- These suspensions were stirred for 2 days before filtering through 1.0 μm filter.
- 30 mg of P3HT were dissolved in 1 mL of chlorobenzene for 8h before filtering through 0.45 μm filter.
- Each ZnO solution sample was mixed with P3HT solution. These solutions were calculated using 26 vol% ZnO. This value was reported as the optimum ratio for this photovoltaic type [13].

5.2.3.3 Photovoltaic fabrication

- Poly(3,4-ethylenedioxythiophene):poly(styrenesulfonate) (PEDOT: PSS) (Baytron P) (PEDOT: PSS: DI water ratio of 1:1) was deposited on ITO glasses by spin coating at 4000 rpm for 40 sec.
- These samples were dried at 80°C for 15 min. Then, the ZnO/P3HT solution was spin coated onto the PEDOT: PSS layer at 1500 rpm.
- Lithium fluoride (LiF) (Aldrich) and aluminum (Al) (Sigma-Aldrich) electrodes were evaporated on the samples in a

Denton DV 502 vacuum chamber at approximately 3–4 Å and 100 nm thick, respectively.

- The devices were annealed in a dry nitrogen glovebox using direct contact with a hot plate at 150 °C for 3 min.

Schematic cross-sectional view of hybrid bulk heterojunction photovoltaic device structure is shown in Figure 5.5. The hybrid bulk heterojunction photovoltaic devices before they were deposited with LiF and Al back electrode were shown in Figure 5.6.

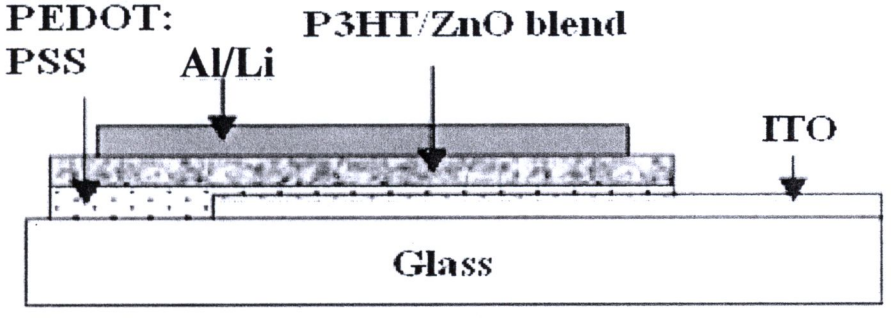

Figure 5.5 The photovoltaic device structure [23]

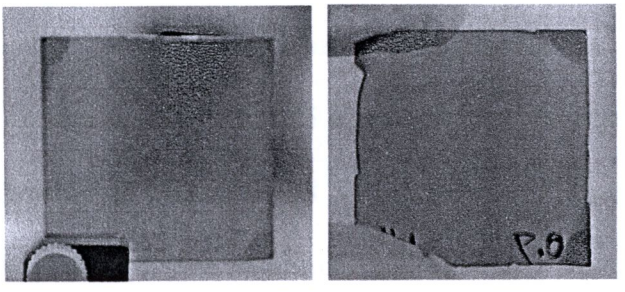

Figure 5.6 The hybrid bulk heterojunction photovoltaic devices before depositing with LiF and Al back electrode

5.3 Results and discussion

In this research pure ZnO and WO_3-doped ZnO nanoparticles synthesized by flame spray pyrolysis were used for replacing conjugated polymer (1-(3-methoxycarbonyl) propyl-1-phenyl [6,6]C_{61}) or PCBM which was widely used in bulk heterojunction photovoltaic as an electron acceptor since PCBM was very expensive. It's 5 times the price of gold. Hybrid ZnO/P3HT bulk heterojunction photovoltaic devices with difference WO_3 concentrations were prepared and investigated by current-voltage characteristic under 1 sun equivalence (1.5 Air mass condition). These current-voltage characteristics were collected using Keithley 236 source-measurement unit.

5.3.1 Characterization of hybrid ZnO/P3HT bulk heterojunction photovoltaic devices

Figure 5.7 shows the current-voltage (I-V) characteristic of hybrid pure ZnO/P3HT photovoltaic measured under AM 1.5 illumination. It was found that the current value of this device was negative and quite stable when it was applied by a voltage in the range of -1.5 to 0 V. At 0 volt bias, the current was 0.299 mA. The short circuit current (I_{SC}) could be found by dividing the current at this point with the active area. Therefore, I_{SC} of this device equaled to 0.974 mA/cm^2. When the voltage applied on this device was higher than 0.25 V, the current was rapidly increased until the curve crossed the voltage axis at 0.708 V. The voltage at this crossed point was the open-circuit voltage (V_{OC}). The maximum power (volt x current) from the curve in the fourth quadrant is called the maximum deliverable power (V_mI_m). From this curve, V_mI_m value equaled to 0.315 mW. The fill factor (FF) which was corresponded to V_mI_m as shown in equation 5.1 was 0.457. The power conversion efficiency (η) that

reflects how good the photovoltaic can convert light to electrical current could be calculated using equation 5.2. For this device, the power conversion efficiency equaled to 0.315 %.

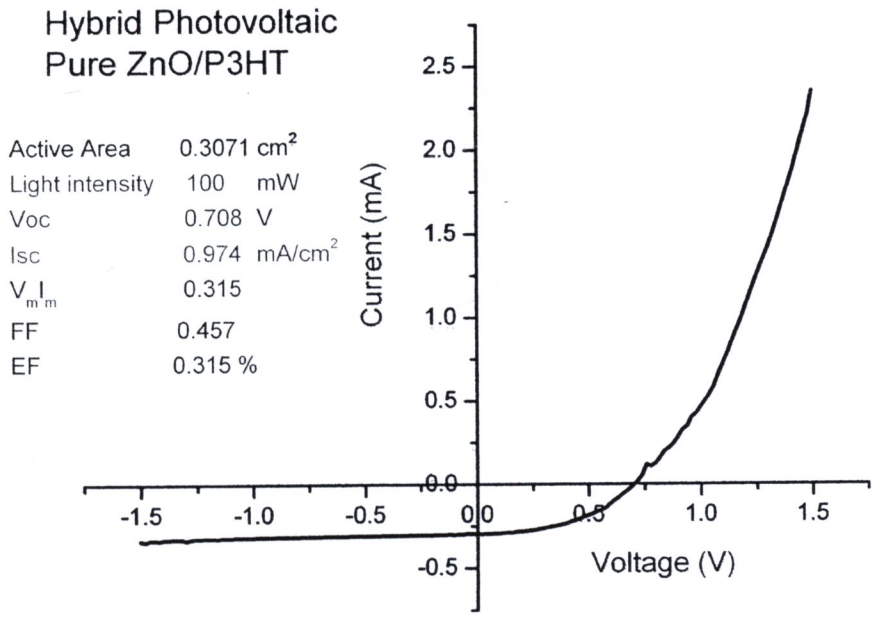

Figure 5.7 The current-voltage (I-V) characteristic of hybrid pure ZnO/P3HT photovoltaic measured under AM 1.5 illumination

Likewise, Figure 5.8-5.12 show I-V characteristic of hybrid 0.25, 0.50, 0.75, 1.0 and 3.0 mol% WO_3-doped ZnO/P3HT photovoltaic measured under AM 1.5 illumination. At 0 volt bias, the current were 0.329, 0.384, 0.381, 0.362 and 0.381 mA, respectively. I_{SC} were 1.07, 1.25, 1.24, 1.18 and 1.24 mA/cm^2, respectively. When the voltage applied on these devices was higher than 0.25 V, the current was rapidly increased until the curve crossed the voltage axis. Therefore, the V_{OC} were 0.713, 0.706, 0.681, 0.673 and 0.641, respectively. V_mI_m equaled to 0.324, 0.411, 0.354, 0.349 and 0.306 mW, respectively. FF which were corresponded to V_mI_m as shown in equation 5.1 were 0.427, 0.465, 0.421, 0.421 and 0.406, respectively. The

power conversion efficiency (η) equaled to 0.324, 0.411, 0.354, 0.349 and 0.306%, respectively. The values of V_{OC}, I_{SC}, V_mI_m, FF and η(%) were listed in Table 5.1.

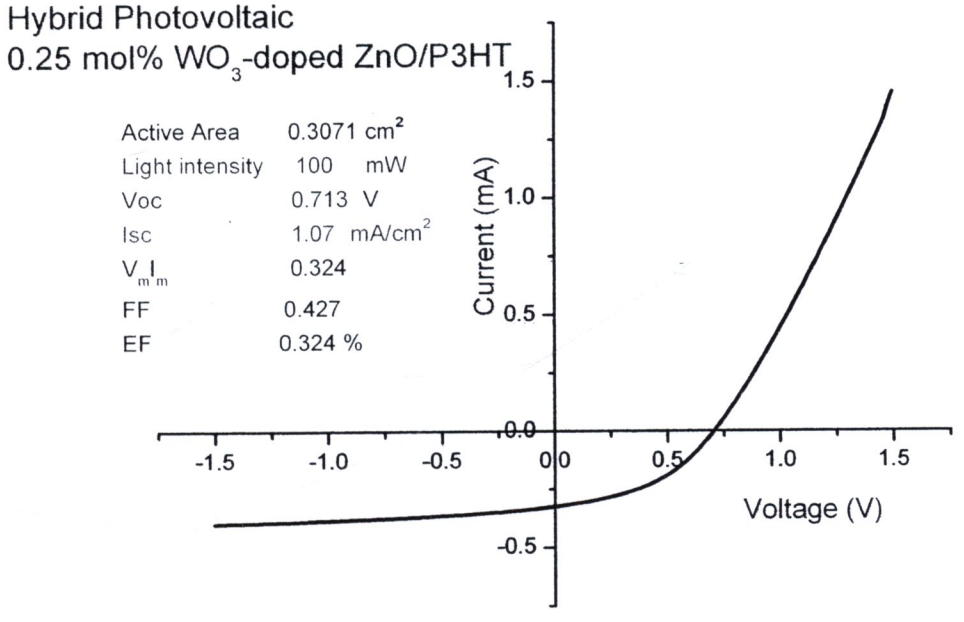

Figure 5.8 The current-voltage (I-V) characteristic of hybrid 0.25 mol% WO_3-doped ZnO/P3HT photovoltaic measured under AM 1.5 illumination

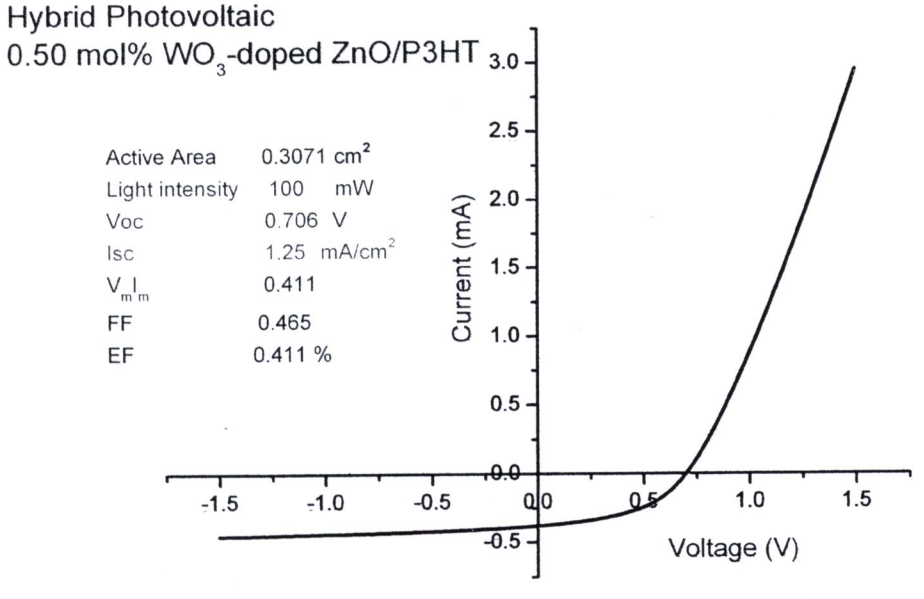

Figure 5.9 The current-voltage (I-V) characteristic of hybrid 0.50 mol% WO_3-doped ZnO/P3HT photovoltaic measured under AM 1.5 illumination

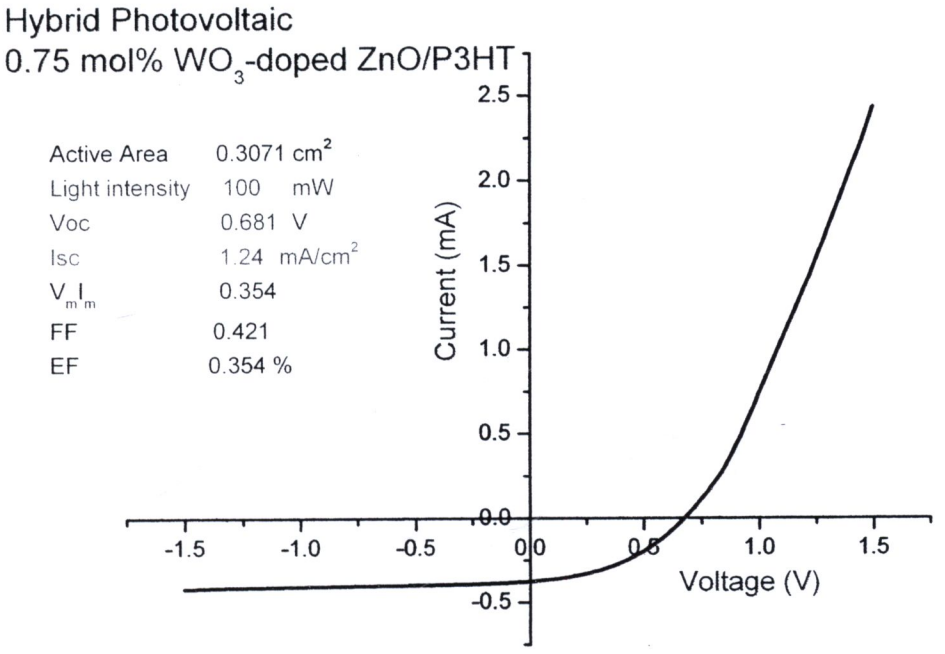

Figure 5.10 The current-voltage (I-V) characteristic of hybrid 0.75 mol% WO_3-doped ZnO/P3HT photovoltaic measured under AM 1.5 illumination

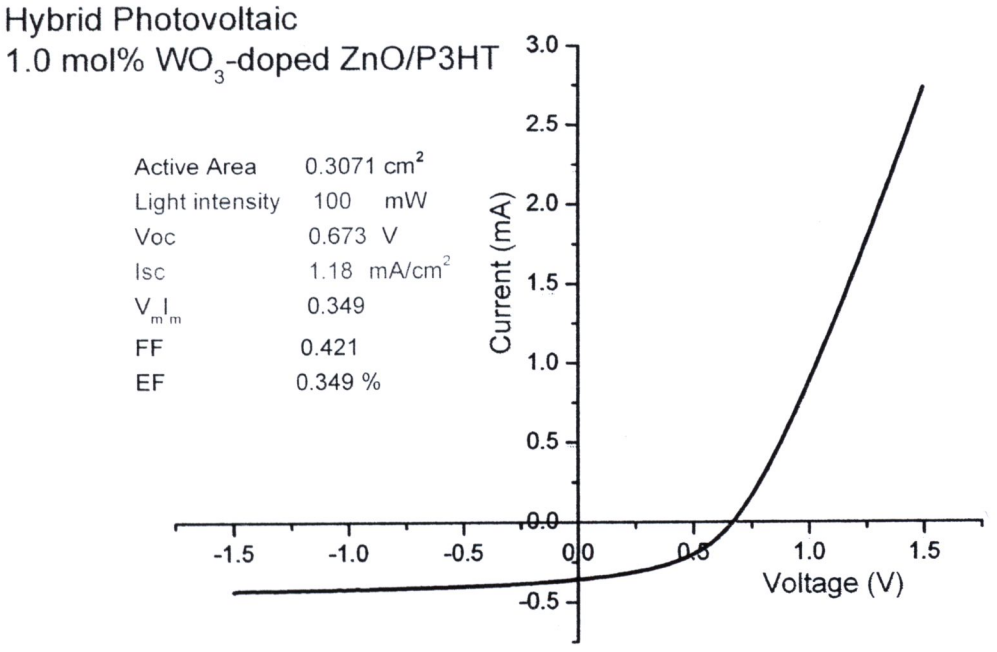

Figure 5.11 The current-voltage (I-V) characteristic of hybrid 1.0 mol% WO_3-doped ZnO/P3HT photovoltaic measured under AM 1.5 illumination

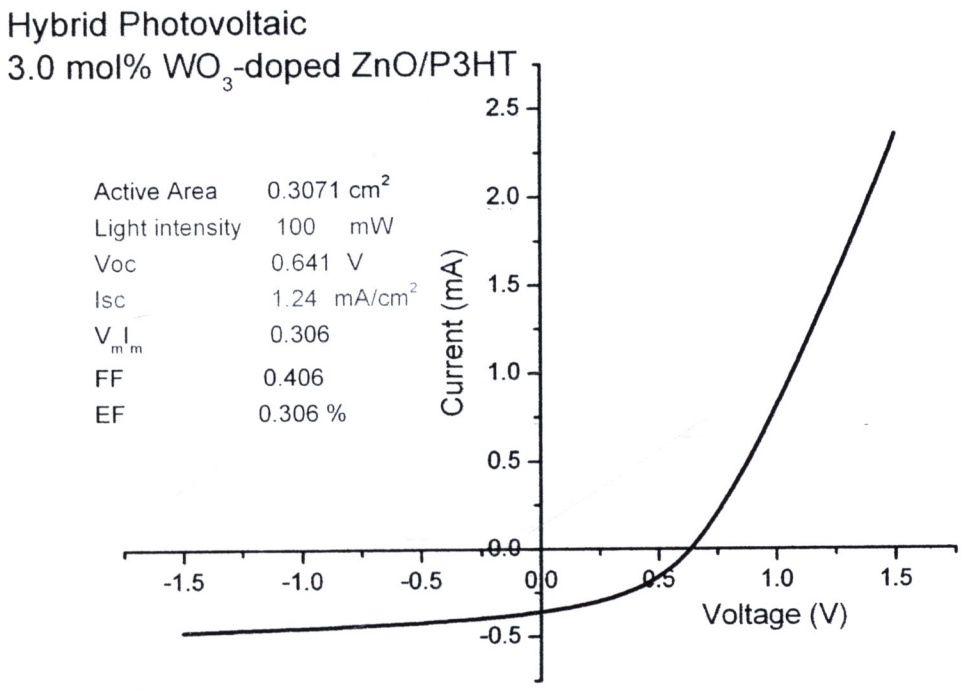

Figure 5.12 The current-voltage (I-V) characteristic of hybrid 3.0 mol% WO_3-doped ZnO/P3HT photovoltaic measured under AM 1.5 illumination

The comparison of current-voltage (I-V) characteristic of hybrid WO_3-doped ZnO/P3HT photovoltaic with difference WO_3 concentration was shown in Figure 5.13. It was found that I_{SC} of all hybrid photovoltaic devices using WO_3-doped ZnO as an electron acceptor were higher than that of hybrid photovoltaic device using pure ZnO. Moreover, the areas under curves in the fourth quadrant of 0.25-1.0 mol% WO_3-doped ZnO/P3HT photovoltaic devices were bigger than that of pure ZnO/P3HT photovoltaic device. Especially, 0.50 mol% WO_3-doped ZnO/P3HT photovoltaic device showed the biggest area under curve in the fourth quadrant. As we know, the more area under curve is, the higher power conversion efficiency will get. Therefore, the optimum amount of WO_3 doping in hybrid WO_3-doped ZnO/P3HT photovoltaic was 0.50 mol%.

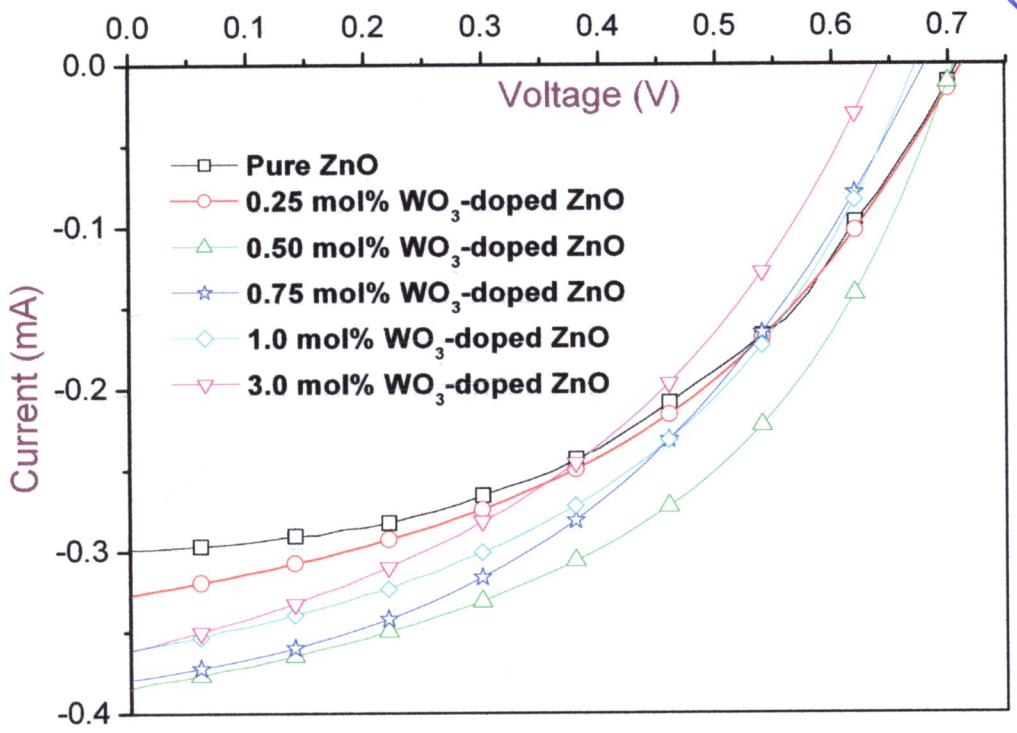

Figure 5.13 The comparison of current-voltage (I-V) characteristic of hybrid WO_3-doped ZnO/P3HT photovoltaic with difference amount of WO_3 concentration

The characteristic parameters of hybrid WO_3-doped ZnO/P3HT photovoltaic with difference WO_3 concentration were concluded in Table 5.1. It was found that the highest V_{OC} was shown by hybrid photovoltaic that used 0.25 mol% WO_3-doped ZnO as an electron acceptor, while the highest I_{SC} was shown by hybrid photovoltaic that used 0.50 mol% WO_3-doped ZnO as an electron acceptor. This suggests that there is an effect due to the WO_3 which improves the number of photons that are actually converted to charge carriers. The fill factors of all devices were in the same range of 0.40-0.47. Moreover, hybrid 0.50 mol% WO_3-doped ZnO/P3HT photovoltaic was the best device that got the highest power conversion efficiency of to 0.411%. This power conversion efficiency value is comparable with Janssen's value of 0.9% [13].

Table 5.1 Characteristic parameters of hybrid WO_3-doped ZnO/P3HT photovoltaic with different WO_3 concentration

Mol % of WO_3-doped ZnO	V_{OC} (V)	I at V=0V (mA)	I_{SC} (mA/cm^2)	V_mI_m (mW)	FF	η (%)
0	0.708	0.299	0.974	0.315	0.457	0.315
0.25	0.713	0.329	1.07	0.324	0.427	0.324
0.50	0.706	0.384	1.25	0.411	0.465	0.411
0.75	0.681	0.381	1.24	0.354	0.421	0.354
1.0	0.673	0.362	1.18	0.349	0.421	0.349
3.0	0.641	0.381	1.24	0.306	0.406	0.306

5.4 Conclusions

The pure ZnO and WO_3-doped ZnO nanoparticles synthesized by flame spray pyrolysis were successfully applied in hybrid photovoltaic devices as an electron acceptor. The current-voltage characteristic of these devices showed that WO_3 could increase the number of photons actually converted to charge carriers which affect the power conversion efficiency. These results could be concluded that an appropriate amount of WO_3 doping could enhance the hybrid photovoltaic efficiency. Especially, hybrid ZnO/P3HT photovoltaic device with 0.50 mol% WO_3-doped ZnO as an electron acceptor exhibited maximum power conversion efficiency of 0.411%.

REFERENCES

1. Jager-Waldau A. *PV Status Report 2008*, European Commission, EUR 23604, EN.
2. Petritsch, K. *Organic Solar Cell Architectures*, Ph. D. Thesis, Technische Universität Graz, Austria, 2000.
3. Shockley W., Queisser H.J. Detailed balance limit of efficiency of PN junction solar cells, *J.Appl.Phys.*, 1961, **32**, 510-519.
4. Lewerenz, H.J., Jungblut, H. *Photovoltaic-Grundlagen und Anwendungen*, Springer, New York,1995.
5. Halls J.M., Walsh C.A., Greenham N.C., Marseglia E.A., Friend R.H., Moratti S.C., Holmes A.B. Efficient photodiodes from interpenetrating polymer networks, *Nature*, 1995, **376**, 498-500.
6. Yu G., Gao J., Hummelen J.C., Wudl F., Heeger A.J. Polymer Photovoltaic Cells: Enhanced Efficiencies via a Network of Internal Donor-Acceptor Heterojunctions, *Science*, 1995, **270**, 1789-1791.
7. Peumans P., Yakimov A., Forrest S.R., Small molecular weight organic thin-film photodetectors and solar cells, *J. Appl. Phys.*, 2003, **93**, 3693-3723.
8. Shaheen E., Brabec C.J., Sariciftci N.S., Padinger F., Fromherz T., Hummelen J.C. 2.5% efficient organic plastic solar cells, *Appl. Phys. Lett.*, 2001, **78**, 841-843.
9. Schilinsky P., Waldauf C., Brabec C.J. Recombination and loss analysis in polythiophene based bulk heterojunction photodetectors, *Appl. Phys. Lett.*, 2002, **81**, 3885-3887.

10. Wienk M.M., Kroon J.M., Verhees W.J.H., Hummelen J.C., Van-Hal P.A., Janssen R.A.J. Efficient Methano[70] fullerene/MDMO-PPV Bulk Heterojunction Photovoltaic Cells, *Angew. Chem. Int. Ed.*, 2003, **42**, 3371- 3375.

11. Huynh W.U., Dittmer J.J., Alivisatos A.P. Hybrid Nanorod-Polymer Solar Cells, *Science*, 2002, **295**, 24252427.

12. Sun B., Marx E., Greenham N.C. Photovoltaic Devices Using Blends of Branched CdSe Nanoparticles and Conjugated Polymers, *Nano Lett.*, 2003, **3**, 961-963.

13. Beek W.J.E., Wienk M.M., Janssen R.A.J. Hybrid Solar Cells from Regioregular Polythiophene and ZnO Nanoparticles, *Adv. Funct. Mater.*, 2006, **16**, 1112-1116.

14. O'Regan B., Grätzel M. A low-cost, high-efficiency solar cell based on dye-sensitized colloidal TiO_2 films, *Nature*, 1991, **353**, 737-740.

15. Hagfeldt A., Grätzel M. Molecular Photovoltaics, *Accounts Chem. Res.*, 2000, **33**, 269-277.

16. Roest A. L., Kelly J.J., Vanmaekelbergh D., Meulenkamp E.A. Staircase in the Electron Mobility of a ZnO Quantum Dot Assembly due to Shell Filling, *Phys. Rev. lett.*, 2002, **89**, 036801(1)- 036801(4).

17. Kiezke T. Recent Advances in Organic Solar Cells, *Adv. Optoelectron.*, 2007, **2007**, 1-15.

18. Jazairli M.A.K. *Groth of Zinc Oxide Nanoparticles on Top of Polymer and Organic Small Molecules as a Transparent Cathode in Tandem Photovoltaic Device*, Ph. D. Thesis, Linkoping University, Sweden 2008.

19. Liu J., Namboothiry M.A.G., Carroll D.L. Roles of donor and acceptor nanodomains in 6% efficient thermally annealed polymer photovoltaics, *Appl. Phys. Lett.*, 2007, **90**, 163511(1)- 163511(3).

20. Kim J.Y., Lee K., Coates N.E., Moses D., Nguyen T.Q., Dante M., Heeger A.J. Efficient Tandem Polymer Solar Cells Fabricated by All-Solution Processing, *Science*, 2007, **317**, 222-225.

21. Brabec C.J., Shaheen S.E., Winder C., Sariciftci N.S., and Denk P. Effect of LiF/metal electrodes on the performance of plastic solar cells, *Appl. Phys. Lett.*, 2002, **80**, 1288-1290.

22. Roman L.S., Mammo W., Petterson L.A.A., Andersson M.R., Inganas O. High quantum efficiency polythiophene/C60 photodiodes., *Adv. Mater.*, 1998, **10**, 774-778.

23. Beek W.J.E., Wienk M.M., Janssen R.A.J. Efficient hybrid solar cells from zinc oxide nanoparticles and a conjugated polymer, *Adv. Mater.*, 2004, **16**, 1009-1013.

24. Bouclé J., Ravirajanac P., Nelson J. Hybrid polymer–metal oxide thin films for photovoltaic applications, *J. Mater. Chem.*, 2007, **17**, 3141–3153.

25. Greenham N.C., Peng X., Alivisatos A.P. Charge separation and transport in conjugated-polymer/semiconductor-nanocrystal composites studied by photoluminescence quenching and photoconductivity, *Phys. Rev. B.*, 1996, **54**, 628-237.

26. Wang H., Oey C.C., Djurišić A.B., Xie M.H., Leung Y.H., Man K.K.Y., Chan W.K., Pandey A., Nunzi J.M., Chui P.C., Titania bicontinuous network structures for solar cell applications, *Appl. Phys. Lett.*, 2005, **87**, 023507(1)- 023507(3).

27. Kudo N., Honda S., Shimazaki Y., Ohkita H., Ito S., Benten H., Improvement of charge injection efficiency in organic-inorganic hybrid solar cells by chemical modification of metal oxides with organic molecules, *Appl. Phys. Lett.*, 2007, **90**, 183513(1)-183513(3).

28. Gilot J., Barbu I., Wienk M.M., Janssen R.A.J. The use of ZnO as opticle spaceer in polymer solar cells: Theoretical and experimental study, *Appl. Phys. Lett.*, 2007, **91**, 113520(1)-113520(3)